Parametric modelling of radiation forces for hybrid wind-wave energy converters

Maria Luisa Celesti, Nicolás Faedo, and Giuliana Mattiazzo

***Abstract*— Mathematical models for design, optimisation, and control of hybrid wind-wave energy conversion systems are of fundamental importance to support their cost-effective development. While numerical solvers can be exploited to compute a characterisation of the hydrodynamical behaviour, these provide non-parametric representations, generating both computational and representational difficulties, manifested through convolution operators linked to radiation effects. Motivated by the necessity of computing parametric models for hybrid wind-wave devices, and the inherent complexity in achieving this task successfully, this paper proposes a radiation parameterisation procedure based on the theory of rational interpolation. Considering a benchmark wind-wave energy conversion system, an approximating state-space model is computed using a Loewner-based approach to replace the radiation convolution operator, using only the raw information available from hydrodynamic codes. The resulting parametric model is analysed extensively, both in the frequency and time domains, including a variety of sea state conditions.**

I. Introduction

Hybrid systems combining multiple renewable sources have emerged as a promising solution for improving the reliability and efficiency of energy production [1]. In particular, the integration of wind and wave energy technologies enables better resource complementarity and higher capacity factors compared to single-source systems. Such hybrid configurations can reduce intermittency, optimise power output, and make more effective use of offshore infrastructures. However, their design and control pose significant challenges due to the coupling between different physical domains and the complexity of the underlying dynamics.

In this context, mathematical modelling of hybrid wind-wave energy systems is of immeasurable value towards advancing these technologies: from performance assessment and geometry optimisation [2], to development of control/estimation algorithms for optimal energy absorption [3], [4], the availability of mathematical models plays an integral role, endowing the industrial and academic communities with an improved understanding on the behaviour of these hybrid devices in diverse operating conditions. Such mathematical representations can be exploited to simulate these hybrid systems in hypothetical situations, before effectively incurring the high costs associated with prototyping, supporting a systematic development protocol.

A particularly challenging aspect of modelling these hybrid converters arises when representing hydrodynamic behaviour. Even in the widely-adopted linear conditions, *i.e.* within the framework of so-called linear potential flow theory, the characterisation of these hydrodynamic effects has to be performed numerically, leading to non-parametric representations (see *e.g.* [5], [6]). In particular, the response associated with the fluid-body interaction is computed using hydrodynamic codes at a finite set of points (virtually always in the frequency domain), based on boundary element methods (BEMs) [7]. These are widely available, including commercial and open source variants.

The non-parametric nature arising from the use of BEMs automatically introduces the necessity of solving convolution operations in the time domain [5]. A particularly relevant convolution, which dictates the internal (force-to-motion) behaviour of the hybrid wind-wave energy converter, is linked to the so-called *radiation* forces, which represent fluid memory effects. Being constrained to solve this convolution numerically has several consequences, including an elevated computational cost and a representational incompatibility with standard control/estimation/optimisation procedures [8], which normally require parametric (closed-form) mathematical models for effective design and synthesis. While this parametric representation for relatively simple floating bodies can be achieved with a reasonable accuracy using off-the-shelf techniques (see *e.g.* [9]), hybrid wind-wave energy systems present complex higher-order interactions between platform and WEC, further exacerbated by the complexity associated with the geometry of each independent body (and corresponding modes of motion).

Motivated by the intrinsic necessity of computing parametric models for hybrid wind-wave energy conversion devices, and the inherent complexity in achieving this task successfully, this paper proposes a radiation parameterisation procedure based on the theory of rational (system) interpolation [10]. In particular, using a benchmark wind-wave energy conversion system, featuring an offshore wind turbine and a flap-type WEC, an approximating state-space model is computed using a Loewner-based approach, to replace the radiation convolution operator, using only the raw information available from BEM codes. The provided parametric model, which is guaranteed to comply with all the physical properties associated with radiation effects, is analysed extensively, both in the frequency and time domains, including a variety of different irregular wave conditions.

The remainder of this paper is organised as follows. Section I-A introduces the main notation used in this study. Section II presents the fundamentals underpinning hydrodynamic modelling of hybrid wind-wave devices, while Section

[1]Maria Luisa Celesti, Nicolás Faedo, and Giuliana Mattiazzo are with the Marine Offshore Renewable Energy Lab, Department of Mechanical and Aerospace Engineering, Politecnico di Torino, Turin, Italy. marialuisa.celesti@polito.it

III introduces the Loewner-based interpolation procedure. Section IV provides an in-depth numerical appraisal of the computed radiation model for the chosen benchmark system, in both frequency and time domains. Finally, Section V outlines the main conclusions arising from this study.

A. Notation

The symbol 0 stands for any zero element, dimensioned according to the context, while $\mathbb{I}_n$ denotes the identity in $\mathbb{C}^{n\times n}$. The transpose of a matrix $A \in \mathbb{C}^{m\times n}$ is denoted as $A^{\mathsf{T}} \in \mathbb{C}^{n\times m}$. Given a function $f(t)$, $t \in \mathbb{R}$, its Laplace transform (provided it exists) is denoted as $F(s)$, $s = \varsigma + \jmath\omega \in \mathbb{C}$, $\{\varsigma, \omega\} \subset \mathbb{R}$. With some abuse of notation, its Fourier transform is denoted as the restriction of F on $\jmath\mathbb{R}$, *i.e.* $F(\jmath\omega)$. The convolution between two functions $\{f, g\}$ (provided it exists) is denoted as $(f * g)(t) = \int_{-\infty}^{t} f(\tau)g(t-\tau)\mathrm{d}\tau$.

II. Hydrodynamic modelling

Within this section, the fundamentals underpinning hydrodynamic modelling for hybrid wind-wave energy systems are briefly recalled. In particular, the benchmark concept presented in [11] is considered, illustrated herein within Figure 1. The device features a floating offshore wind turbine with a semi-submersible triangular platform (composed of three pillars), and a flap-type WEC system, hinged to the front beam. The device is designed to have the flap WEC facing the dominant wave direction.

Fig. 1. Schematic representation of the analysed hybrid wind-wave energy converter (left), and corresponding hydrodynamic panel mesh used for the BEM analysis below the still water level (right).

Considering that the hybrid converter is represented in terms of $m \in \mathbb{N}$ degrees-of-freedom (DoFs), a standard form of the motion equation focusing on the hydrodynamic loads can be derived as follows:

$$M\ddot{q} + f_{\text{rest}}(q) + f_{\text{visc}}(\dot{q}) + f_{\text{rad}}(\ddot{q}, \dot{q}) = f_{\text{ext}}(q, \dot{q}, t), \quad (1)$$

where $q(t) \in \mathbb{R}^m$ denotes the generalised position vector of the body. $M \in \mathbb{R}^{m\times m}$ is the generalised inertia-mass matrix, f_{rest} indicates restoring effects resulting from the difference between gravity and buoyancy forces, while f_{visc} represents viscous damping. The term f_{rad} accounts for radiation forces due to wave-induced fluid motion generated by body oscillations and depends on both the instantaneous and past time history of the motion, leading to memory effects. Finally, f_{ext} includes wave excitation forces (*i.e.* wave diffraction and dynamic Froude-Krylov forces), and incorporates control inputs and other external components.

The radiation term $f_{\text{rad}}(\ddot{q}, \dot{q})$ is typically modelled in the linear potential flow theory framework via the so-called Cummins equation [12]. This formulation separates the radiation force into two components, *i.e.*

$$f_{\text{rad}}(\dot{q}) = a_\infty \ddot{q} + k * \dot{q} \equiv a_\infty \ddot{q} + f_{\text{rad}}^{\text{conv}}, \quad (2)$$

where $a_\infty \in \mathbb{R}^{m\times m}$ is the so-called added-mass at infinite frequency, and the impulse response function $k \in L^2(\mathbb{R}^{m\times m})$, involved in the convolution operator in (2), is the kernel characterising the fluid memory effect.

The map k, which defines a causal linear time-invariant system $k : \dot{q} \mapsto f_{\text{rad}}^{\text{conv}}$, is commonly characterised in terms of its associated frequency-response function K, defined in terms of the so-called hydrodynamic coefficients as:

$$K(\jmath\omega) = b(\omega) + \jmath\omega\left(a(\omega) - a_\infty\right), \quad (3)$$

with $b(\omega) \in \mathbb{R}^{m\times m}$ the radiation damping and $a(\omega) \in \mathbb{R}^{m\times m}$ the radiation added-mass.

Though linear, the characterisation of the radiation subsystem as in (3) is performed numerically, by exploiting BEM solvers (as discussed within Section I). These hydrodynamic codes, which are widely available (both in commercial and open-source versions - see [7]), compute $b(\omega)$ and $a(\omega)$ for a finite set of ω values using a mesh of the overall floating structure (see Figure 1 - right), while also offering an estimation of a_∞. In other words, $K(\jmath\omega)$ is only known at a finite set of (user-defined) frequencies, hence being intrinsically non-parametric.

Relying only on the raw BEM output, time-domain simulation/characterisation of the hybrid wind-wave energy converter can only be performed by computing the discrete inverse Fourier transform of K, and subsequently solving the convolution map in (2) numerically. This has, at least, three significant drawbacks: (a) numerically solving the convolution requires a sufficiently accurate representation of $k(t)$, which in turn requires a more refined frequency-domain definition within BEM codes, increasing the computational effort; (b) direct integration of $k * \dot{q}$ is highly inefficient in computational terms and; (c) the non-parametric nature of K (equivalently k) complicates design and synthesis of standard control/estimation techniques, which virtually always require a closed-form differential equation describing the hybrid system motion. As discussed within the introduction, one can resort to a parametric approximation for k, in terms of a suitable dynamical structure $\tilde{k}$. This is addressed explicitly within Section III, exploiting a Loewner-based approach.

III. Parametric approximation

This section briefly recalls the fundamental elements underpinning the so-called Loewner framework, originally developed within [10]. The core of this technique is based on the notion of interpolation: using the frequency-domain data computed with BEM solvers, as per equation (3), one aims to find an approximating parametric dynamical system able to achieve interpolation at a user-defined set of data, *i.e.*

$$\text{left: } \ell_j^{\mathsf{T}} \tilde{K}(\jmath\mu_j) = v_j^{\mathsf{T}}, \quad \text{right: } \tilde{K}(\jmath\lambda_i) r_i = w_i, \tag{4}$$

with $j \in \mathbb{N}_k$, $j \in \mathbb{N}_q$, and where the triples $(\ell_j, \jmath\mu_j, v_j)$ and $(r_j, \jmath\lambda_j, w_j)$ represent the so-called *left* and *right* interpolation datasets. Note that, once the sets of left and right frequencies, $\mathscr{F}_\ell = \{\mu_i\}_{i\in\mathbb{N}_k}$ and $\mathscr{F}_r = \{\lambda_i\}_{i\in\mathbb{N}_q}$, respectively, are defined, the associated pairs (ℓ_i, v_i) and (r_i, w_i) follow directly from (3). In particular, one can simply choose the right and left directions $\{r_i, \ell_i^{\mathsf{T}}\} \subset \mathbb{R}^m$ as columns/rows of the identity matrix accordingly, and their corresponding columns/rows in the matrix $K(\jmath\omega) \in \mathbb{C}^{m\times m}$ as v_i and w_i, hence filling the required response data.

With the left and right datasets, the associated *Loewner* $\mathbb{L}$ and *shifted Loewner* $\mathbb{L}_s$ matrices can be defined [10], conforming the so-called *Loewner pencil*, as follows:

$$\begin{aligned} \mathbb{L} &= \begin{bmatrix} \frac{v_1^{\mathsf{T}} r_1 - \ell_1^{\mathsf{T}} w_1}{\mu_1 - \lambda_1} & \cdots & \frac{v_1^{\mathsf{T}} r_k - \ell_1^{\mathsf{T}} w_k}{\mu_1 - \lambda_k} \\ \vdots & \ddots & \vdots \\ \frac{v_q^{\mathsf{T}} r_1 - \ell_q^{\mathsf{T}} w_1}{\mu_q - \lambda_1} & \cdots & \frac{v_q^{\mathsf{T}} r_k - \ell_q^{\mathsf{T}} w_k}{\mu_q - \lambda_k} \end{bmatrix}, \\ \mathbb{L}_s &= \begin{bmatrix} \frac{\mu_1 v_1^{\mathsf{T}} r_1 - \ell_1^{\mathsf{T}} w_1 \lambda_1}{\mu_1 - \lambda_1} & \cdots & \frac{\mu_1 v_1^{\mathsf{T}} r_k - \ell_1^{\mathsf{T}} w_k \lambda_k}{\mu_1 - \lambda_k} \\ \vdots & \ddots & \vdots \\ \frac{\mu_q v_q^{\mathsf{T}} r_1 - \ell_q^{\mathsf{T}} w_1 \lambda_1}{\mu_q - \lambda_1} & \cdots & \frac{\mu_q v_q^{\mathsf{T}} r_k - \ell_q^{\mathsf{T}} w_k \lambda_k}{\mu_q - \lambda_k} \end{bmatrix}. \end{aligned} \tag{5}$$

Remark 1: $\mathbb{L}$ and $\mathbb{L}_s$ are well-defined if the sets of left and right interpolation frequencies are disjoint, *i.e.* $\mathscr{F}_\ell \cap \mathscr{F}_r = \emptyset$. With the definition of the Loewner matrices in (5), and being compliant with Remark 1, the system defined by the map

$$\tilde{K} : \mathbb{C} \to \mathbb{C}^{m\times m}, \; s \mapsto \tilde{K}(s) = -W(s\mathbb{L} - \mathbb{L}_s)^{-1} V, \tag{6}$$

where the set of matrices $\{V, W\}$ is given by,

$$V^{\mathsf{T}} = \begin{bmatrix} v_1 & \cdots & v_q \end{bmatrix}, \quad W = \begin{bmatrix} w_1 & \cdots & w_k \end{bmatrix}, \tag{7}$$

interpolates the set of left and right data , *i.e.* fulfills (4) (see [10] for a formal proof).

Note that, depending on the cardinality of the sets $\mathscr{F}_\ell$ and $\mathscr{F}_r$ (*i.e.* the number of frequencies within left and right datasets), achieving exact interpolation as in (6) can require a high-dimensional order parametric model $\tilde{K}$, which might conflict with real-time control requirements. To avoid this potential drawback, and have a direct handle on the final complexity of the approximating model (10), one can resort [10] to the singular value decomposition associated with the Loewner pencil $\xi\mathbb{L} - \mathbb{L}_s$, for all $\xi \in \mathscr{F}_\ell \cup \mathscr{F}_r$, *i.e.*

$$[\mathbb{L} \;\; \mathbb{L}_s] = Y_1 S_1 X_1^{\mathsf{T}}, \quad \begin{bmatrix} \mathbb{L} \\ \mathbb{L}_s \end{bmatrix} = Y_2 S_2 X_2^{\mathsf{T}}, \tag{8}$$

where $Y_1 \in \mathbb{C}^{q\times z}$ and $X_2 \in \mathbb{C}^{k\times z}$. Let $\bar{r} \leq z$ and define the following projected decompositions:

$$Y_1^{\bar{r}} = Y_1 \begin{bmatrix} \mathbb{I}_{\bar{r}} \\ 0 \end{bmatrix}, \quad X_2^{\bar{r}} = X_2 \begin{bmatrix} \mathbb{I}_{\bar{r}} \\ 0 \end{bmatrix}. \tag{9}$$

Leveraging (9), the $\bar{r}$-order parametric system defined by

$$\tilde{K}(s) = -W^{\ddagger}(s\mathbb{L}^{\ddagger} - \mathbb{L}_s^{\ddagger})^{-1} V^{\ddagger}, \tag{10}$$

with the projected matrices

$$\begin{aligned} \mathbb{L}^{\ddagger} &= -Y_1^{\bar{r}\mathsf{T}} \mathbb{L} X_2^{\bar{r}}, \quad & \mathbb{L}_s^{\ddagger} &= -Y_1^{\bar{r}\mathsf{T}} \mathbb{L}_s X_2^{\bar{r}}, \\ V^{\ddagger} &= Y_1^{\bar{r}\mathsf{T}} V, & W^{\ddagger} &= W X_2^{\bar{r}}, \end{aligned} \tag{11}$$

define an (approximate) interpolant of the data.

Remark 2: Complexity, *i.e.* model order, of the data-driven interpolant in (11), is essentially controlled by retaining only the $\bar{r} \leq z$ dominant singular values from the corresponding Loewner pencil. Exact interpolation is recovered by simply setting $\bar{r} = z$.

Assuming that $\mathbb{L}^{\ddagger}$ is invertible[1], it is straightforward to show that equation (10) defines the transfer function of an associated continuous-time system, written, for all $t \in \mathbb{R}$, as

$$\tilde{k} : \begin{cases} \dot{x}(t) = Ax(t) + B\dot{q}(t), \\ y(t) = Cx(t) \approx f_{\text{conv}}^{\text{rad}}(t) \end{cases} \equiv \; \tilde{k}(t) = \Re(Ce^{At}B), \tag{12}$$

with $x(t) \in \mathbb{C}^{\bar{r}}$, and where

$$A = \mathbb{L}^{\ddagger^{-1}} \mathbb{L}_s^{\ddagger}, \quad B = -\mathbb{L}^{\ddagger^{-1}} V^{\ddagger}, \quad C = W^{\ddagger}. \tag{13}$$

Remark 3: Complex-valued matrices (A, B, C) in (12) can be easily avoided altogether by including complex-conjugate data within the sets $\mathscr{F}_\ell$ and $\mathscr{F}_r$. This guarantees the existence of a unitary matrix that maps the Loewner matrices in (5) to a corresponding real form [10].

A. Internal stability and passivity of the interpolants

It is well-known from the general theory of marine structures (see *e.g.* [5]) that the radiation subsystem for a floating body (or interacting bodies - such as the considered hybrid wind-wave system) is both stable and passive. Note that the state-space model derived in (12) does not inherently ensure internal stability, although this property typically holds for suitably chosen model orders $\bar{r}$ in the projection step (9). Nonetheless, in cases in which $\tilde{k}$ exhibits unstable behaviour for a specified model order $\bar{r}$, it is always possible to perform a decomposition into stable and unstable 'parts', $\tilde{k}^+$ and $\tilde{k}^-$, respectively[2], following classical results from linear system theory [13], and hence directly replace $\tilde{k} \leftarrow\!\shortmid \tilde{k}^+$. Once stability has been guaranteed, passivity can be enforced by perturbation of the output matrix C, *i.e.* $C \leftarrow\!\shortmid C + \Delta C$, effectively changing the transmission zeros of (12). The perturbation matrix ΔC is designed to ensure passivity by enforcing the Kalman-Yakubovich-Popov (positive real) lemma, via semi-definite optimisation [6].

[1]This is a reasonable assumption, given the properties of the radiation system (in particular, causality). Nonetheless, if, due to numerical issues, $\mathbb{L}^{\ddagger}$ loses rank, one can simply resort to a generalised inverse.

[2]Note that $\tilde{k}^+$ is the optimal approximation of $\tilde{k}$ in $\mathcal{RH}_2$ [13].

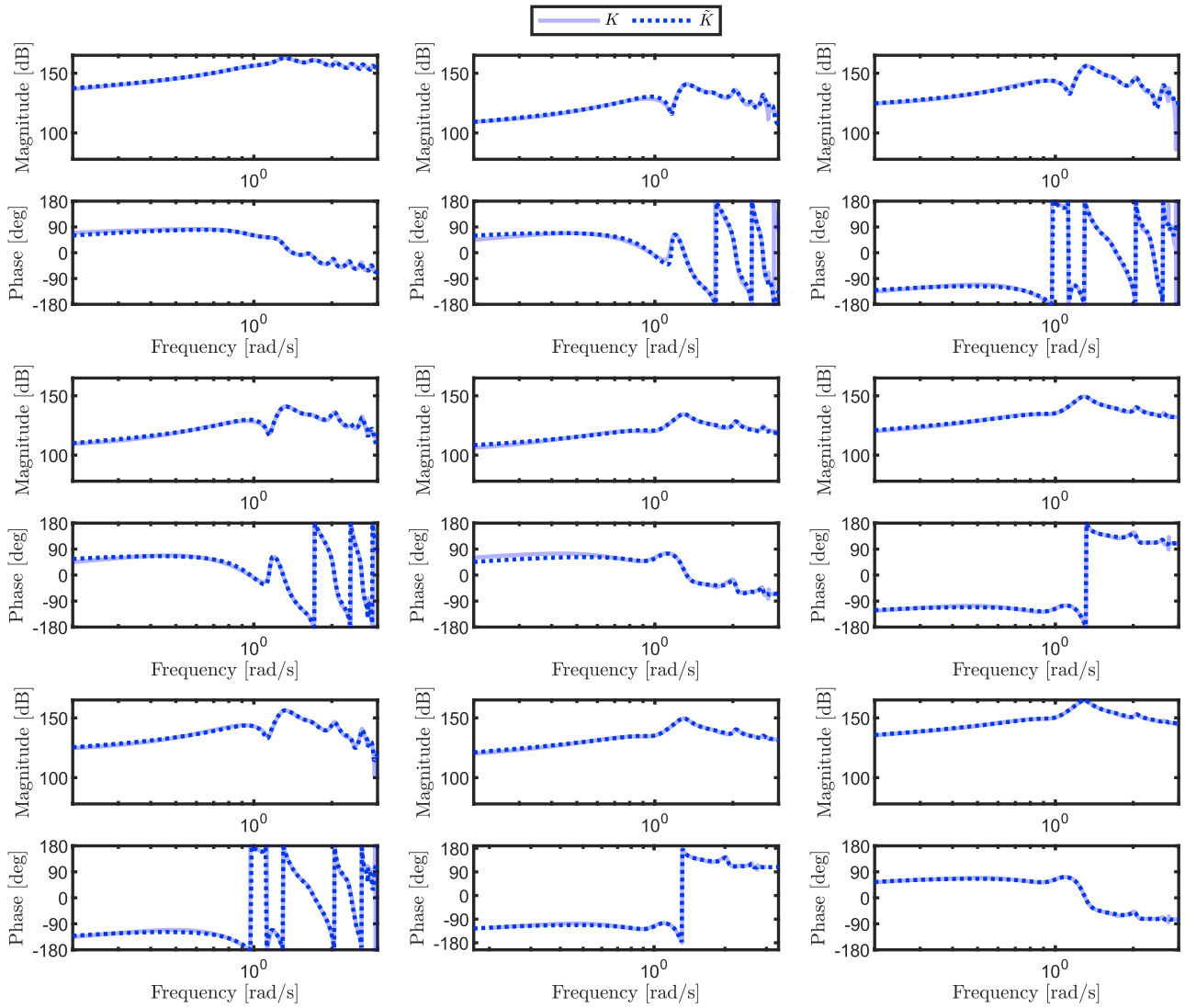

Fig. 2. Bode plot for the frequency response of the radiation system, computed via BEM solver K and the obtained approximation $\tilde{K}$.

IV. Numerical appraisal

Within this section, the hybrid device introduced in Section II is modelled considering the three main relevant DoFs involved in energy conversion (in order): pitch motion of the flap, and surge and pitch of the platform, and hence $m = 3$ in equation (1). Accordingly, the radiation frequency response $K(\jmath\omega) \in \mathbb{C}^{3\times3}$ is non-sparse, fully accounting for cross-coupling hydrodynamic effects between the three considered DoFs. The corresponding hydrodynamic coefficients, used to reconstruct numerically (3), are obtained from BEM simulations, using the solver *Capytaine* [14] interfaced via *BEMRosetta* [15]. The data is computed over a finite frequency range, bounded by a lower limit ω_- and an upper limit ω_+, such that $[\omega_-, \omega_+] \subset \mathbb{R}$.

Regarding the interpolation procedure, as outlined within Section III, the sets of left and right interpolation frequencies are formed using a total of 200 points, following a Chebyshev distribution (of the first kind). Following Remark 3, and to avoid a complex-valued state-space representation for the radiation subsystem, the sets $\mathscr{F}_\ell$ and $\mathscr{F}_r$ (and corresponding responses - see Section III) are expanded to include complex-conjugate information, guaranteeing a system (A, B, C) as in (12) defined over $\mathbb{R}$. The chosen approximation order, via projection based on the singular value decomposition of the corresponding Loewner pencil (see equation (9)), is set to $\bar{r} = 23$. Stability and passivity are enforced as per Section III-A, leading to a physically consistent radiation model.

Figure 2 reports the frequency response of both target K and approximating $\tilde{K}$ radiation systems, in terms of Bode diagrams, showing both magnitude and phase, for each element composing the corresponding frequency-response operator. These curves serve as a reference for evaluating the quality of the Loewner-based parametric approximation $\tilde{K}(\jmath\omega)$. Note that the target radiation, *i.e.* (3), presents a complex response, featuring multiple modes (peaks), generated by the strong interaction between the two bodies (particularly in pitch). Nonetheless, as evident from the Bode plots, the proposed parametric model closely matches the original BEM-based

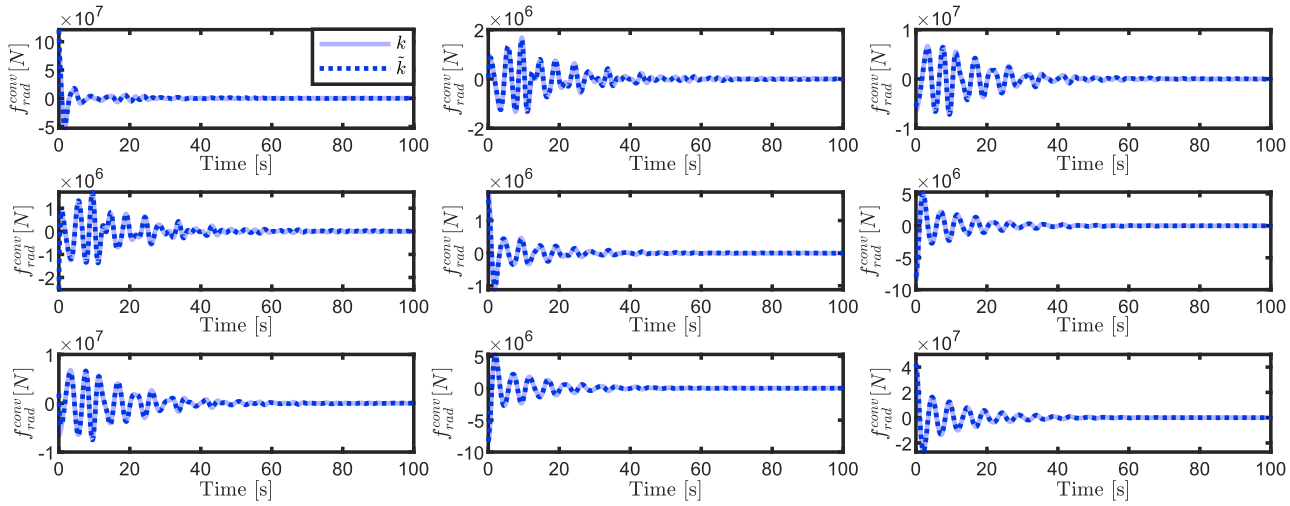

Fig. 3. Target k and approximating $\tilde{k}$ radiation impulse response functions.

mapping across the entire frequency range, virtually overlapping all maxima and minima, following the multimodal nature of the target response.

While Figure 2 highlights the accuracy of the computed parametric model in the frequency domain, ultimately, the objective is to simulate the behaviour of the hybrid wind-wave system in the time domain. As such, and to further validate the performance of the proposed parametric approximation, Figure 3 shows the radiation force response to an impulsive velocity input applied to the system, *i.e.* the target impulse response function k in (2), together with that corresponding to the approximating system $\tilde{k}$ in (12). The results obtained using the original hydrodynamic operator k and its parametric counterpart $\tilde{k}$ are virtually overlapped, confirming that the parametric model accurately captures the transient dynamics of the radiation forces, reinforcing the findings observed in the frequency-domain analysis.

To further demonstrate the time-domain performance of the approximating model computed via Loewner, simulations corresponding to relevant sea state conditions are presented in the following. In particular, velocity inputs generated based on irregular waves following a JONSWAP [16] spectra (see Figure 4), characterised by a peak enhancement factor $\gamma = 3.3$, significant wave height $H_s = 2$ [m], and a peak period T_p defined as the period corresponding to the frequency associated with the $\mathcal{H}_\infty$-norm of target BEM response, are considered. Two additional spectra are also included within the following appraisal, by varying T_p by $\pm 20\%$, to analyse the response under diverse sea state conditions. These spectra are combined with the system frequency-domain model to produce the velocity signals in the frequency domain, which are then transformed to the time domain via inverse Fourier transform. The resulting time-domain velocity inputs are used to evaluate the radiation force responses of both the target and approximating parametric models.

Figure 5 illustrates the radiation force responses for the case where the input velocities correspond to a JONSWAP spectrum with T_p matching the frequency of the system maximum singular value, *i.e.* the $\mathcal{H}_\infty$-norm. The velocities are also displayed for reference, using the right axis. The near-perfect overlap between the force responses obtained from the non-parametric target operator k and the Loewner-based approximation $\tilde{k}$ confirms the accuracy of the approximating model in replicating the system dynamic behaviour under relevant sea state excitation.

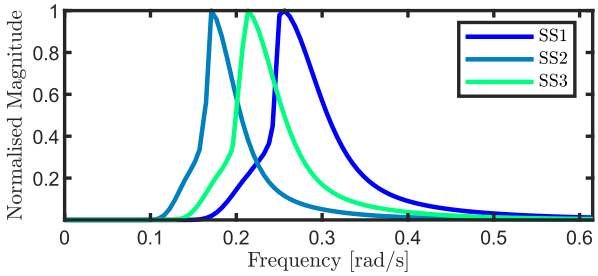

Fig. 4. JONSWAP spectra for the generated waves (and corresponding velocity profiles for simulation), normalised with respect to each maximum.

Finally, and to further extend the results presented in Figure 5, Figure 6 shows the time-domain absolute approximation errors between the output corresponding to the Loewner-based model and the reference hydrodynamic data. The pointwise error is defined as:

$$e(y(t)) = \frac{|y(t) - y_{\text{target}}(t)|}{\max |y_{\text{target}}(t)|}, \tag{14}$$

where y and y_{target} denote the output of the approximating model and that associated with the target BEM data, respectively. Note that the normalisation is performed using the maximum absolute value of the target response over the considered simulation time interval. To provide a comprehensive performance measure, the normalised mean absolute error (NMAE) is also provided, which aggregates the pointwise errors over the entire simulation interval. The results indicate that the parametric Loewner-based model achieves an exceptionally low NMAE (less than $\approx 2\%$), confirming its ability to accurately capture the radiation force dynamics

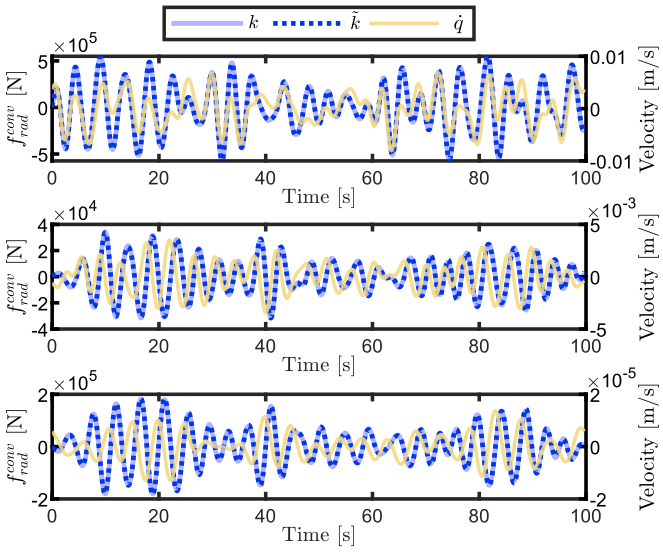

Fig. 5. Time-domain comparison of $f_{\text{rad}}^{\text{conv}}$, computed using the non-parametric BEM-based kernel (solid line) and its parametric approximation (dashed line). The same velocity vector $\dot{q}$ (right axis) is used as input to both models.

with a compact and computationally efficient representation. Notably, the NMAE does not have a significant variation for different sea-states across the considered DoFs, highlighting the overall accuracy of the provided model.

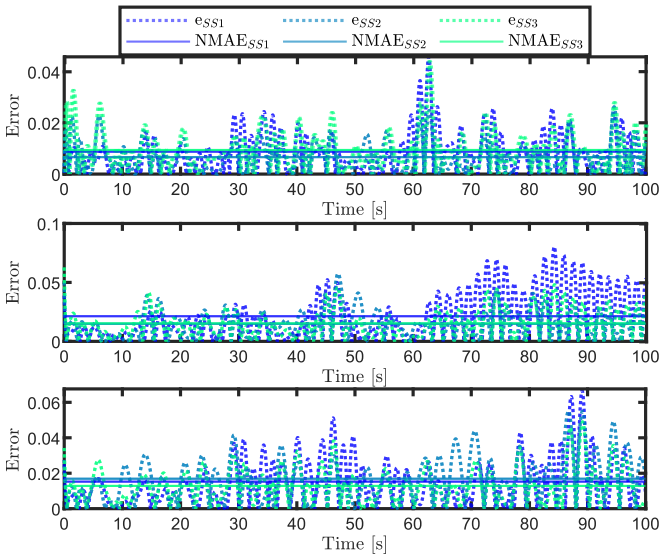

Fig. 6. Normalised error and NMAE between the output associated with the target system and its parametric approximation across the considered degrees of freedom, for each of the considered sea states.

V. Conclusions

This paper presents an interpolation-based procedure for parametric modelling of radiation forces in hybrid wind-wave energy systems. In particular, leveraging a Loewner-based approach, state-space models which are physically consistent (*i.e.* internally stable and passive) are derived, using only raw data readily available from BEM codes. A detailed case study, featuring a floating offshore wind turbine together with a flap-type WEC, is considered for parametric modelling. The results obtained show that the technique presented within this paper is able to represent the complex hydrodynamic interactions characterising such a hybrid device, with an exceptional degree of accuracy, both in the frequency and time domains, featuring an NMAE of less than $\approx 2\%$ for different relevant irregular wave conditions. Future work will exploit the derived mathematical models for computationally efficient geometry optimisation and real-time optimal control of wind-wave energy converters.

References

[1] X. Dong, Y. Li, D. Li, F. Cao, X. Jiang, and H. Shi, "A state-of-the-art review of the hybrid wind-wave energy converter," *Progress in Energy*, vol. 4, no. 4, p. 042004, 2022.

[2] M. L. Celesti, B. Paduano, Y. Peña-Sanchez, E. Pasta, N. Faedo, and J. Ringwood, "Design considerations for a hybrid wind-wave platform under energy-maximising control," in *Proceedings of the European wave and tidal energy conference*, vol. 15, pp. 1–5, European Wave and Tidal Energy Conference EWTEC, 2023.

[3] H. Zhu, "Optimal semi-active control for a hybrid wind-wave energy system on motion reduction," *IEEE Transactions on Sustainable Energy*, vol. 14, no. 1, pp. 75–82, 2022.

[4] M. L. Celesti, N. Faedo, and G. Mattiazzo, "Stabilisation and energy absorption control for wind-wave hybrid platforms: a generalised lqr approach," in *ISOPE International Ocean and Polar Engineering Conference*, pp. ISOPE–I, ISOPE, 2024.

[5] R. Taghipour, T. Perez, and T. Moan, "Hybrid frequency–time domain models for dynamic response analysis of marine structures," *Ocean Engineering*, vol. 35, no. 7, pp. 685–705, 2008.

[6] N. Faedo, Y. Peña-Sanchez, F. Carapellese, G. Mattiazzo, and J. V. Ringwood, "LMI-based passivation of LTI systems with application to marine structures," *IET Renewable Power Generation*, vol. 15, no. 14, pp. 3424–3433, 2021.

[7] L. Papillon, R. Costello, and J. V. Ringwood, "Boundary element and integral methods in potential flow theory: A review with a focus on wave energy applications," *Journal of Ocean Engineering and Marine Energy*, vol. 6, no. 3, pp. 303–337, 2020.

[8] J. V. Ringwood, S. Zhan, and N. Faedo, "Empowering wave energy with control technology: Possibilities and pitfalls," *Annual Reviews in Control*, vol. 55, pp. 18–44, 2023.

[9] T. Perez and T. I. Fossen, "A matlab toolbox for parametric identification of radiation-force models of ships and offshore structures," *Modeling, Identification and Control*, vol. 30, no. 1, pp. 1–15, 2009.

[10] A. Mayo and A. C. Antoulas, "A framework for the solution of the generalized realization problem," *Linear algebra and its applications*, vol. 425, no. 2-3, pp. 634–662, 2007.

[11] M. L. Celesti, B. Paduano, Y. Peña-Sanchez, E. Pasta, N. Faedo, and J. V. Ringwood, "On the behaviour of a combined wind-wave energy conversion platform under energy-maximising control conditions," in *OCEANS 2023-Limerick*, pp. 1–6, IEEE, 2023.

[12] W. Cummins, "The impulse response function and ship motions. schiffstechnik," *Heft*, vol. 47, pp. 101–109, 1962.

[13] M. Köhler, "On the closest stable descriptor system in the respective spaces $\mathcal{RH}_2$ and $\mathcal{RH}_\infty$," *Linear Algebra and its Applications*, vol. 443, pp. 34–49, 2014.

[14] M. Ancellin and F. Dias, "Capytaine: a python-based linear potential flow solver," *Journal of Open Source Software*, vol. 4, no. 36, p. 1341, 2019.

[15] I. Zabala, Y. Pena-Sanchez, T. Kelly, J. Henriques, M. Penalba, N. Faedo, J. Ringwood, and J. M. Blanco, "BEMRosetta: An open-source hydrodynamic coefficients converter and viewer integrated with nemoh and FOAMM," in *European Tidal and Wave Energy Conference Proceedings*, 2021.

[16] K. Hasselmann, T. P. Barnett, E. Bouws, H. Carlson, D. E. Cartwright, K. Enke, J. Ewing, A. Gienapp, D. Hasselmann, P. Kruseman, *et al.*, "Measurements of wind-wave growth and swell decay during the joint north sea wave project (JONSWAP).," *Ergaenzungsheft zur Deutschen Hydrographischen Zeitschrift, Reihe A*, 1973.